Research Article

3.6 W compact all-fiber Pr³⁺-doped green laser at 521 nm

Jinhai Zou[a,b] Jinfen Hong,[a,b] Zhuang Zhao,[c] Qingyuan Li,[a] Qiujun Ruan,[a] Hang Wang,[a] Yikun Bu,[a,*] Xianchao Guan,[c] Min Zhou,[c] Zhiyong Feng,[c] and Zhengqian Luo[a,b,d,*]

[a]Xiamen University, School of Electronic Science and Engineering, Fujian Key Laboratory of Ultrafast Laser Technology and Applications, Xiamen, China
[b]Innovation Laboratory for Sciences and Technologies of Energy Materials of Fujian Province (IKKEM), Xiamen, China
[c]Huawei Technologies Co., Ltd., Shenzhen, China
[d]Xiamen University, Shenzhen Research Institute, Shenzhen, China

Abstract. Green semiconductor lasers are still undeveloped, so high-power green lasers have heavily relied on nonlinear frequency conversion of near-infrared lasers, precluding compact and low-cost green laser systems. Here, we report the first Watt-level all-fiber CW Pr³⁺-doped laser operating directly in the green spectral region, addressing the aforementioned difficulties. The compact all-fiber laser consists of a double-clad Pr³⁺-doped fluoride fiber, two homemade fiber dichroic mirrors at visible wavelengths, and a 443-nm fiber-pigtailed pump source. Benefitting from $> 10~\mathrm{MW/cm^2}$ high damage intensity of our designed fiber dielectric mirror, the green laser can stably deliver 3.62-W of continuous-wave power at ~521 nm with a slope efficiency of 20.9%. To the best of our knowledge, this is the largest output power directly from green fiber lasers, which is one order higher than previously reported. Moreover, these green all-fiber laser designs are optimized by using experiments and numerical simulations. Numerical results are in excellent agreement with our experimental results and show that the optimal gain fiber length, output mirror reflectivity, and doping level should be considered to obtain higher power and efficiency. This work may pave a path toward compact high-power green all-fiber lasers for applications in biomedicine, laser display, underwater detection, and spectroscopy.

Keywords: fiber laser; high power; Pr³⁺-doped fiber; green light.

1 Introduction

Green lasers are of great interest in biomedicine, laser display, spectroscopy, underwater optical communications, and scientific research.[1] In contrast to the well-developed red or blue laser diodes (LDs), LDs emitting directly in the green region are still under development and hence the "green gap" exists.[2] Currently, the leading technology for producing high-power continuous-wave (CW) green lasers is still the nonlinear frequency conversion (e.g., frequency doubling) of near-infrared solid-state or fiber laser systems,[3,4] and the compactness, stabilization, and expenditure are still challenges. As a result, researchers are

always looking for an alternate green-light laser solution that has the benefits of great brightness, compactness, and cost-effectiveness. Due to intrinsic advantages, such as good beam quality, small footprint, user-friendliness, and low- to no-maintenance, green fiber lasers doped with trivalent rare-earthions (e.g., Pr³⁺,[5] Ho³⁺,[6] Er³⁺[7]) can satisfy these demands and bridge the "green gap," so there is a huge drive to develop compact high-power rare-earth-doped fiber lasers in the green spectral region.

Given recent advances in both rare-earth-doped fluoride fibers and blue GaN LD, frequency down conversion fiber lasers using trivalent rare-earth-doped fluoride fibers have emerged as a promising approach to directly generate visible-light emission, and much related work has been carried out and reported.[8–14] Among them, Pr³⁺-doped fluoride fiber laser is particularly

appealing for visible lasers because it has a reasonably simple 4f-energy level scheme and exhibits a variety of transitions in the blue, green, orange, and red spectral regions.[8] At present, based on double-clad (DC) Pr^{3+}-doped fluoride fiber, the high-power red fiber laser operating at 635.5 nm with a maximum output power of 2.3 W has been achieved.[13] However, the green Pr^{3+}-doped fiber laser remains rather challenging due to the relatively modest optical gain in the green region, and only a few instances of progress have been reported.[15–17] Okamoto et al. demonstrated in 2011 an all-fiber laser operating at 521 nm with a maximum power of 322 mW through the splicing of a Pr^{3+}-doped fluoride fiber to a silica fiber pigtail mirror.[15] Meanwhile, Nakanishi et al. announced a Pr^{3+}-doped fluoroaluminate single-clad fiber laser delivering 598 mW at 522.2 nm pumped by two space-coupling GaN LDs.[16] In the latter scenario, further utilizing the pulsed pumping, a quasi-CW laser generated a pulse peak power of 1.53 W at 522.2 nm with a slope efficiency of 33.8%.[17] However, up to now, the reported green fiber lasers have not reached Watt-level power output in the CW regime. What is more, all of the high-power green fiber lasers reported previously had used some free-space bulk components in those cavities, which sacrifices the all-fiber structure and undermines the reliability and robustness of the fiber lasers. Therefore, the development of a compact all-fiber green laser with high output power is highly anticipated.

Herein, we designed and experimentally demonstrated a compact high-power all-fiber CW Pr^{3+}-doped green laser for the first time to our knowledge. To begin, an efficient butt-coupled all-fiber structure capable of high-power operation was constructed using a DC Pr^{3+}-doped fluoride fiber treated by the cutting process and fiber dichroic mirrors (FDMs) with

a high damage intensity. Following that, to achieve high-efficiency emission and high-power output, we explored the effects of gain fiber length and output mirror reflectivity on green laser power scaling via experiments and numerical simulations. Finally, according to the optimization results, we designed and further presented an experimental study on the compact high-power green all-fiber laser, which comprises a 2.1-m DC Pr^{3+}-doped fluoride fiber, two FDMs at visible wavelengths, and a 443-nm fiber-pigtailed pump source. The laser can directly generate a 3616-mW green laser output with a central wavelength of ~521 nm and a slope efficiency of 18.8%.

2 Experimental Principle and Setup

2.1 Spectroscopy of DC Pr^{3+}-Doped Fluoride Fiber

First, we briefly discuss the spectroscopic properties of DC Pr^{3+}-doped fluoride fiber. The fiber is manufactured by Le Verre Fluoré and has the following features: a Pr^{3+} doping concentration of 8000 ppm, a 7.5-μm core diameter, a 0.08-numerical aperture (NA) of fiber core, 115/125-μm inner cladding (double D-shaped), and 180-μm outer cladding diameter, respectively. The core cutoff wavelength of this gain fiber is 780 nm, and its V-parameter (normalized frequency) at 521 nm is about 3.6. We first measured the fiber attenuation spectrum (including doping absorption in the core and propagation loss in the inner cladding) at room temperature by a tungsten halogen lamp and a 350- to 1750-nm optical spectrum analyzer (OSA, AQ6315B, Ando), as shown in the inset of Fig. 1(a). The propagation loss spectrum is then estimated by fitting the data at different wavelengths (i.e., 1.10 dB/m at 543 nm, 0.88 dB/m

Fig. 1 Spectroscopy of 8000 ppm DC Pr^{3+}-doped fluoride fiber. (a) Absorption spectrum; inset: attenuation and propagation loss spectra. (b) Absorption cross section spectrum. (c) Simplified energy-level scheme of Pr^{3+}. (d) Fluorescence spectrum excited by a 443-nm laser.

at 650 nm, and 0.74 dB/m at 793 nm) [see the blue curve in the inset of Fig. 1(a)]. Finally, the ground state absorption of DC Pr³⁺-doped fiber is obtained by deducting the propagation loss spectrum from the attenuation spectrum, as shown in Fig. 1(a). The peak absorption coefficient is 2.4 dB/m at 441 nm, while the absorption coefficient at our pump wavelength (i.e., 443 nm) is 2.1 dB/m. The absorption cross sections can be calculated based on Beer–Lambert's law, and the related calculation equations are simply derived as follows:[18,19]

$$\sigma_a(\lambda) = \frac{\alpha(\lambda)}{\Gamma(\lambda) \times N}, \tag{1}$$

$$\Gamma(\lambda) = 1 - \exp\left(-2\frac{a^2}{\omega_0^2}\right), \tag{2}$$

where $\alpha(\lambda)$ and $\Gamma(\lambda)$ are the absorption coefficient and power filling factor of the gain fiber, respectively. N represents the doping concentration of rare-earth ions in the gain fiber. For 8000 ppm DC Pr³⁺-doped fluoride fiber, it has a value of 1.55×10^{26} m⁻³. In addition, a and ω_0 are the core radius and mode field radius of the gain fiber, respectively. According to Eqs. (1) and (2), the absorption cross sections of DC Pr³⁺-doped fluoride fiber are calculated as shown in Fig. 1(b). Note that the absorption cross sections at 441 and 443 nm are 1.01×10^{-24} m² and 0.84×10^{-24} m², respectively.

The simplified energy level scheme of Pr³⁺ for visible fluorescence emission is shown in Fig. 1(c). The frequency down conversion fluorescence emission in the green spectral region is known to emanate from the ³P₁ + ¹I₆ levels. The excitation process is as follows: (1) ³P₂ level is excited by ground state absorption of the ³H₄ level with the ~443 nm pump, (2) nonradiative relaxation from ³P₂ to ³P₁ + ¹I₆, and (3) radiative transition from ³P₁ + ¹I₆ to ³H₅, which can generate fluorescence emission at ~521 and ~536 nm.[20] Figure 1(d) shows the fluorescence emission spectrum of the 0.6-m DC Pr³⁺-doped fluoride fiber excited by a 443-nm laser. The stimulated emission spectrum displays the emission lines in the deep red (~717 nm), red (~635 nm), orange (~603 nm), green (~521 nm), and blue (~480 nm) spectral regions, implying the potential of these different visible-wavelength fiber lasers. In addition, the emission cross sections are computed using the Füchtbauer–Ladenburg (F-L) theory, which is expressed as[21,22]

$$\sigma_e(\lambda) = \frac{1}{8\pi} \frac{\lambda^5 \beta}{n^2 c \tau} \frac{I(\lambda)}{\int I(\lambda)\lambda \cdot \mathrm{d}\lambda}, \tag{3}$$

where λ, β, n, c, and τ are the center wavelength, fluorescence branching ratio from ³P₁ to ³H₅ transition, core refractive index of the gain fiber, light speed, and radiative lifetime of upper laser energy level, respectively. $I(\lambda)$ denotes the intensity of the emission spectrum. The stimulated emission cross section for 521 nm (³P₁ → ³H₅) can be calculated as 0.32×10^{-24} m². Here, we considered a radiative lifetime τ (³P₁) of 40 μs[20] and an experimental fluorescence branching ratio β of 3.2%.

2.2 Experimental Setup

To construct an effective butt-coupled all-fiber structure capable of high-power operation in our experiment, we must first prepare the high-performance FC/PC fiber connectors at both ends of DC Pr³⁺-doped fluoride fiber. At present, due to fragile mechanical properties of fluoride fiber, it is inevitable that the fiber end-facet will be damaged to some extent by the traditional polishing processing [see Fig. 2(a)], which leads to the lower damage intensity of the fiber end-facet and blocks high-power operation. Therefore, to enable visible high-power laser operation, a new reliable processing technology for fluoride fiber end-facet nondestructive processing must be developed. Continuous experiments have revealed that fluoride fiber cutting technology based on a commercial fiber cleaver (CT104+, Fujikura) combined with the fabrication technology of a standard FC/PC fiber connector can effectively solve the aforementioned issues. First, the fiber cleaver is used to cleave the fluoride fiber to obtain the fiber end-facet with high smoothness. The fiber is then inserted into the ceramic core with an inner diameter of 180 μm until it is parallel to the end-facet of the ceramic core. Finally, a small amount of UV-curing adhesive is added to the end of the ceramic core for curing, and the DC Pr³⁺-doped fluoride fiber connector with high smoothness is successfully prepared, as shown in Fig. 2(b). The above process skillfully applies the fiber cutting technology to fabricate the high-quality fluoride fiber connector and ensures the construction of an effective all-fiber structure capable of high-power operation. Furthermore, to obtain high-performance FDMs at visible wavelengths, heat-resistant epoxy resin combined with
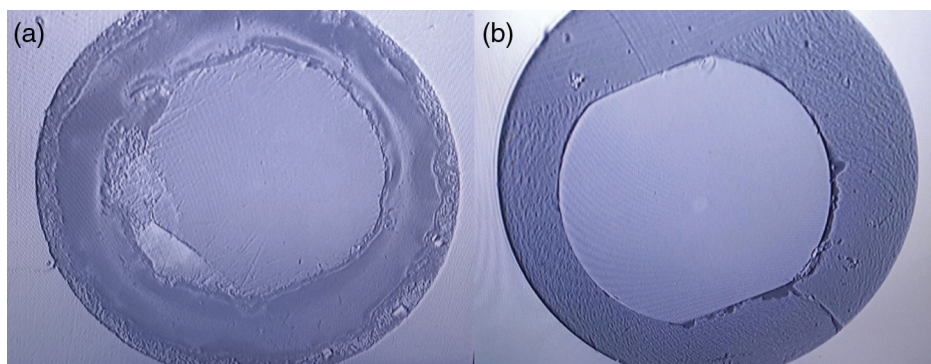
Fig. 2 Microscopic images of DC Pr³⁺-doped fluoride fiber end-facet. (a) Traditional polishing processing and (b) cutting processing.

grinding and polishing technology is first utilized to produce fiber end-facets with high stability and smoothness. The main processes are as follows: (1) producing the silica fiber connector by using the ceramic core and heat-resistant epoxy resin; (2) solidifying the fiber connector at high temperature; and (3) grinding and polishing the end-facet of the solidified fiber connector by a commercial polishing machine. The FDMs at visible wavelengths with high laser damage intensity (> 10 MW/cm^2) are then successfully prepared using an ion beam-assisted deposition system and a specific electric field manipulation of film layers, which is also one of the key factors for achieving high-power green all-fiber lasers.

After finishing the processing of the fluoride fiber connector and the preparation of FDMs with high damage intensity, we designed the all-fiber Pr^{3+}-doped green laser. The schematic of green laser is shown in Fig. 3(a), and Fig. 3(b) shows the corresponding photograph. This laser consists of a DC Pr^{3+}-doped fluoride fiber, two FDMs, and a 443-nm pump source. The pump can deliver 20-W pump power at 443 nm through a standard multimode 105/125-μm (0.22 NA) silica fiber pigtail. Two ceramic sleeves with a 2.5-mm inner diameter are used to realize the low-loss all-fiber coupling between the DC Pr^{3+}-doped fluoride fiber and the visible FDMs. The compact fiber linear cavity for green-light oscillation is constructed by two homemade FDMs (M$_1$, M$_2$). The FDM was fabricated by directly coating the dielectric films onto the end-facet of standard multimode silica fiber. The reflectivity of M$_1$ is as high as 99.7% at 521 nm, and it has a high transmittance of 95.4% at 443 nm [see Fig. 3(c)]. The reflectivity of M$_{2-1}$ and M$_{2-2}$ is 74.9% and 87.2% at 521 nm, respectively, and both have a high reflectivity of >95% at 443 nm [see Fig. 3(c)], which ensures the sufficient utilization of the residual pump laser. All FDMs are designed to have a >90% high transmittance at 635 nm to suppress red laser emission. The propagation loss of the pump laser through the DC Pr^{3+}-doped fluoride fiber is measured to be 1.45 dB/m [see the inset of Fig. 1(a)], whereas the loss of the core is estimated to be ∼0.4 dB/m at 521 nm.[10] In addition, the green laser

was measured by the OSA (AQ-6315E, Ando), and the output power was recorded by a 350- to 1100-nm optical power meter (S425C-L, Thorlabs, Inc.).

3 Results and Discussion

3.1 High-Power All-Fiber Green Laser

According to the optimization results, a ∼2.1-m DC Pr^{3+}-doped fluoride fiber and M$_{2-2}$ were employed for the high-power all-fiber green laser experiment. Figure 4 exemplifies the output characteristics of the green laser. The threshold of the CW green laser is about 1030 mW. Figure 4(a) shows the green output power at different pump powers. With the increase of pump power, the output power increases linearly without saturation, and the slope efficiency is 18.8%. Accordingly, a maximum output power of 3616 mW was attained pumped at 20.01 W. The wide range of the output spectrum at 5.71 W pump power is shown in Fig. 4(b). Note that the central wavelength of the spectrum is 521.2 nm, and the intensity of the green laser is >24 dB higher than that of the residual pump laser, indicating that > 99% of the output laser is green laser. The spectra of the green laser under different pump powers are given in Fig. 4(c). With the increase of pump power, the center wavelength of the green laser shows a slight redshift, and the 3-dB spectral bandwidth also expands. Under strong pumping, the green laser oscillates at multiple wavelengths and has a wide spectral bandwidth due to the design of a high Q cavity in a wide reflective waveband [see Fig. 4(c)]. As shown in Fig. 4(d), to evaluate the operation stability of the all-fiber green laser, we monitored the power curve of the green laser operating at 3.0 W for over 60 min. The intensity fluctuation is <1.0%, showing the excellent long-term stability of the laser operation. In addition, the laser intensity distribution and M^2 factors of the generated green fiber laser beam were measured by a beam quality analyzer (WinCamD-UCD12, DataRay), and the measurement results are shown in the inset of Fig. 4(d). The measured M$^2_{x,y}$
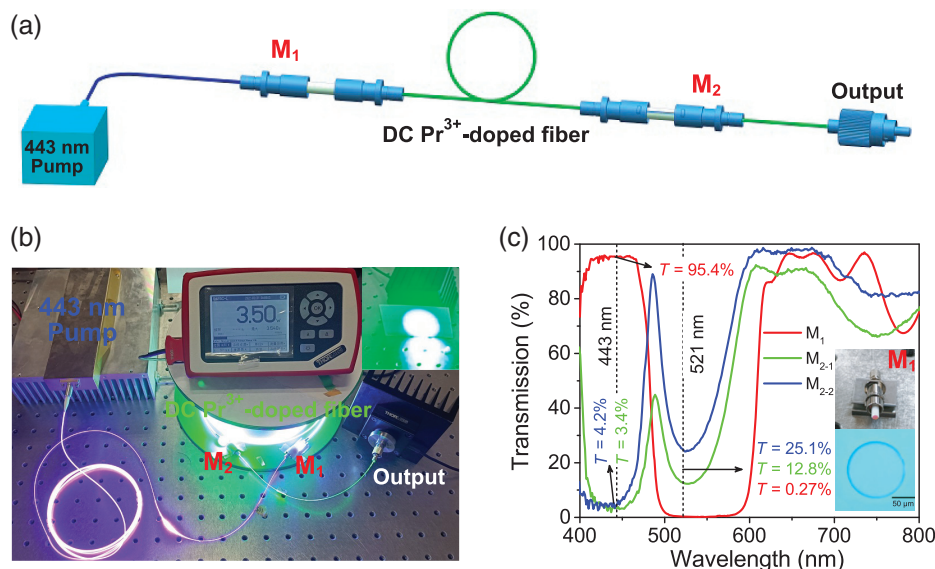
Fig. 3 (a) Schematic and (b) photograph of the compact all-fiber Pr^{3+}-doped green laser (inset: green light laser spot). (c) The transmission spectra of FDMs (M$_1$, M$_2$); insets: photograph (upper) and microscopic image (lower) of the M$_1$.
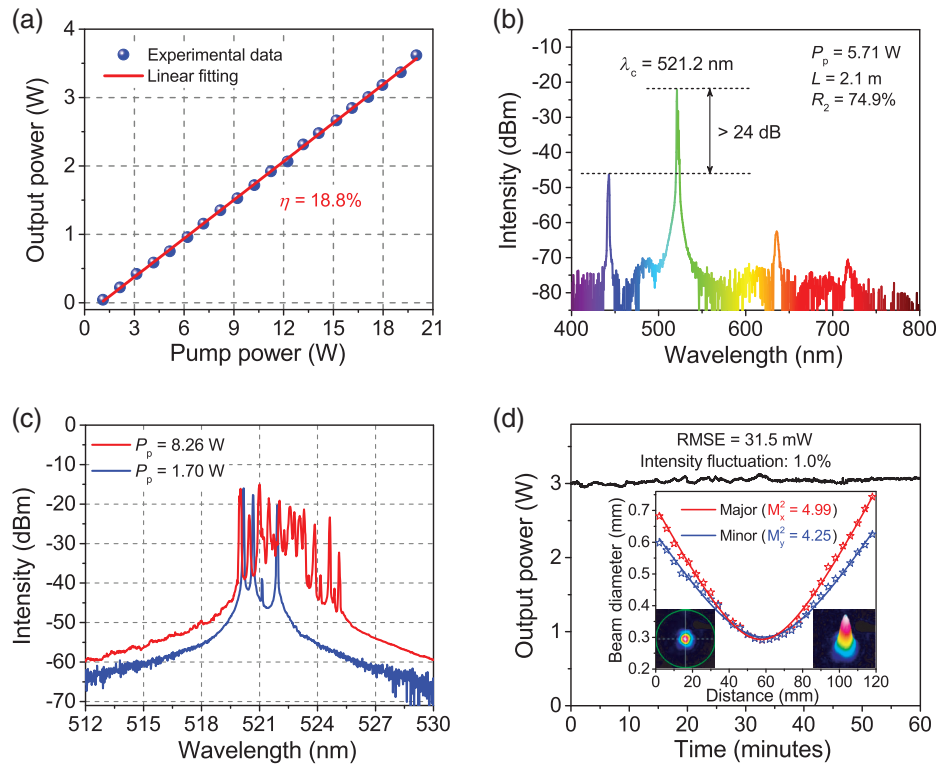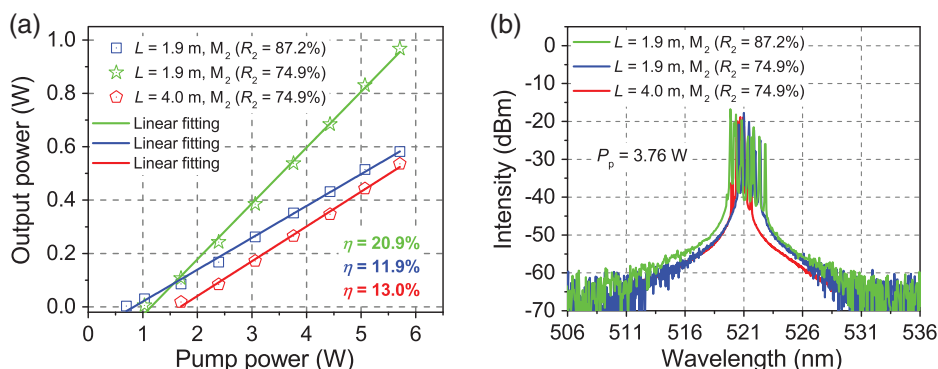
Fig. 4 Characteristics of the high-power all-fiber green laser. (a) Output green power versus the pump power. (b) Typical spectrum collected from 400 to 800 nm under 5.71 W pump power. (c) Output spectra under different pump powers. (d) Power stability curve of the green laser operating at 3.0 W. Insets: the beam quality parameters and intensity distribution of the green laser.

parameters are 4.99 and 4.25, respectively, indicating that the green fiber laser is multitransverse mode operation.

3.2 Output Characteristics of All-Fiber Green Lasers with Different Designs

The output characteristics of the all-fiber green lasers with different designs were investigated experimentally, as shown in Fig. 5. Figure 5(a) shows the green laser power versus the pump power with the different gain fiber lengths (L) and the laser reflectivity (R_2) of M_2. For the R_2 reflectivity of 74.9%, varying the gain fiber from 4 to 1.9 m, both the green output power and

slope efficiency increase from 536 to 830 mW pumped at 5.07 W and from 13.0% to 20.9%, respectively. When $L = 1.9$ m, with R_2 decreasing from 87.2% to 74.9%, both the green output power and slope efficiency increase from 801 to 1344 mW pumped at 7.63 W and from 11.9% to 20.9%, respectively. Figure 5(b) shows the corresponding green spectra pumped at 3.76 W. The results show that all the all-fiber green lasers with different designs oscillate at multiple wavelengths under strong pumping. Along with higher green power, the linewidth of the green laser becomes broadening and new wavelengths are emitted at the edge of the fluorescence spectrum. According to the comparison experiment with different

Fig. 5 Characteristics of the all-fiber green laser with different designs. (a) Output green power versus the pump power and (b) the corresponding spectra pumped at 3.76 W.

designs, the output performance of the all-fiber green laser with ~2.0-m DC Pr³⁺-doped fiber and ~25% output coupling is superior.

3.3 Numerical Analysis

To better understand and further optimize the performance of the all-fiber Pr³⁺-doped green laser, numerical simulations of this laser were carried out. The laser transition process of ~521 nm in Pr³⁺ is a typical four-level system, which can be simulated using the numerical model of the strongly pumped quasi-four-level laser system, as shown in Fig. 6. This model focuses on the correlation transitions among the four energy levels of Pr³⁺ [i.e., $^3H_4$ (N_0), $^3P_0$ (N_3), $^3P_1$ (N_2), and $^3H_5$ (N_1)]. In this case, the steady-state rate equations and power transmission equations can be expressed as follows:[23–25]

$$\frac{N_2(z)}{N} = \frac{\frac{[P_p^+(z)+P_p^-(z)]\sigma_{ap}\Gamma_p}{h\nu_p A_c} + \frac{[P_s^+(z)+P_s^-(z)]\sigma_{as}\Gamma_s}{h\nu_s A_c}}{\frac{[P_p^+(z)+P_p^-(z)](\sigma_{ap}+\sigma_{ep})\Gamma_p}{h\nu_p A_c} + \frac{1}{\tau} + \frac{[P_s^+(z)+P_s^-(z)](\sigma_{es}+\sigma_{as})\Gamma_s}{h\nu_s A_c}}, \tag{4}$$

$$\pm\frac{dP_p^\pm(z)}{dz} = -\Gamma_p[\sigma_{ap}N - (\sigma_{ap}+\sigma_{ep})N_2(z)]P_p^\pm(z) - \alpha_p P_p^\pm(z), \tag{5}$$

$$\pm\frac{dP_s^\pm(z)}{dz} = \Gamma_s[(\sigma_{es}+\sigma_{as})N_2(z) - \sigma_{as}N]P_s^\pm(z) - \alpha_s P_s^\pm(z), \tag{6}$$

where $P_p^+(z)$ [$P_p^-(z)$] and $P_s^+(z)$ [$P_s^-(z)$] are the pump and signal laser powers propagating along the positive (negative) z directions, respectively. ν_p and ν_s are the pump and signal frequency. σ_{ap} (σ_{as}) and σ_{ep} (σ_{es}) represent the absorption and emission cross sections of the pump (signal) laser, respectively. α_p and α_s are the loss coefficients of the pump and signal laser. Γ_p and Γ_s are the power filling factors of the pump and signal laser. A_c is the cross sectional area of the fiber core. The boundary conditions of the end-pumped fiber laser can be written as follows:

$$P_p^+(0) = P_p^l + R_{1p} \cdot P_p^-(0), \tag{7}$$

$$P_p^-(L) = P_p^r + R_{2p} \cdot P_p^+(L), \tag{8}$$

Table 1 The parameters used in numerical simulation.

Parameter	Value	Parameter	Value
λ_p	443 nm	α_p	345.4×10^{-3} m⁻¹
λ_s	521 nm	α_s	92.1×10^{-3} m⁻¹
σ_{ap}	0.84×10^{-24} m²	Γ_p	3.61×10^{-3}
σ_{ep}	0	Γ_s	0.92
σ_{as}	0	L	Variable
σ_{es}	0.32×10^{-24} m²	R_{1p}	4%
τ	40 μs	R_1	99%
N	1.55×10^{26} m⁻³	R_{2p}	95%
A_c	44.2×10^{-12} m²	R_2	Variable

$$P_s^+(0) = R_1 \cdot P_s^-(0), \tag{9}$$

$$P_s^-(L) = R_2 \cdot P_s^+(L), \tag{10}$$

where P_p^l and P_p^r are the pump power injected into the gain fiber from the positive (negative) z directions. R_{1p} (R_1) and R_{2p} (R_2) represent the pump (signal) laser reflectivity of the front and back cavity mirrors, respectively. Some of the parameters used in our simulation are calculated based on the measurements of the DC Pr³⁺-doped fluoride fiber (see Fig. 1), and some are obtained from the literature.[10,20] The specific parameters are summarized in Table 1. After obtaining the simulation parameters, the shooting method and bvp4c function are used to solve Eqs. (4)–(10). The numerical results are shown in Figs. 7 and 8.

As visualized in Fig. 7(a), for a fixed input pump power, the laser output power first increases and then falls as the gain fiber length increases. The figure also reveals that with the decrease of R_2, the L of gain fiber realizing the maximum output power becomes longer. Figure 7(b) shows the laser threshold and slope efficiency of the green fiber laser versus the L under $R_2 = 75\%$, $R_{2p} = 95\%$. A maximum slope efficiency is 23.3% at $L = 1$ m, yielding a laser threshold of 0.84 W. For the designed laser ($R_2 = 75\%$, $R_{2p} = 95\%$), although there exists an optimum fiber length (~1 m), sufficient pump absorption should be considered to ensure that the remaining reverse pump laser does not affect the pump source, and the ~2-m gain fiber is thus

Fig. 6 Numerical model. (a) Typical four-level system and (b) schematic of end-pumped fiber laser.
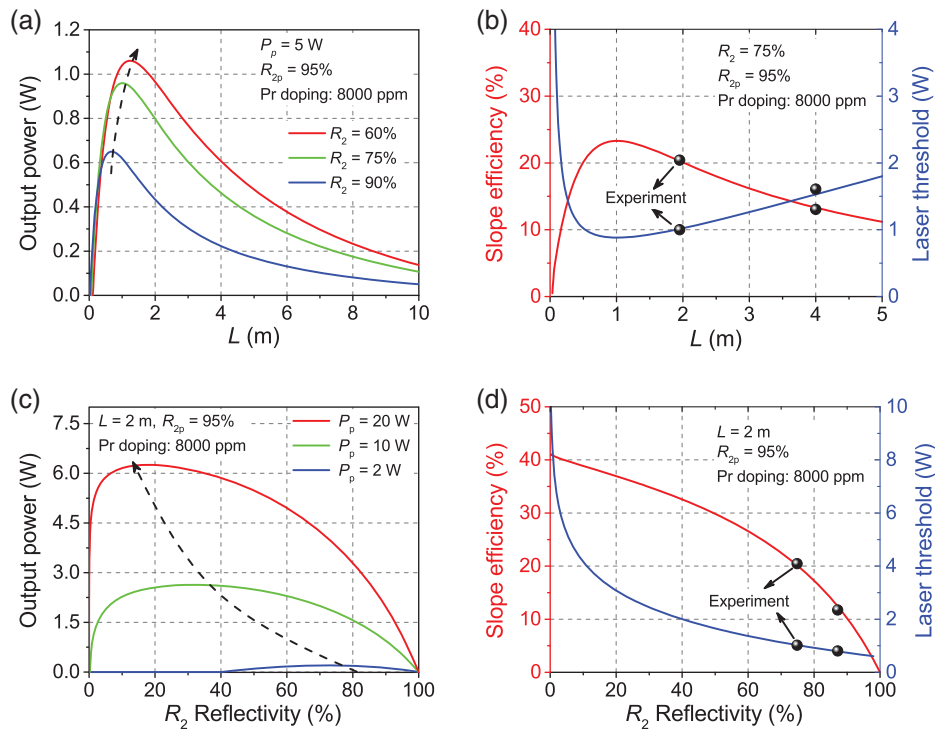
**Fig. 7** Simulation performance of the all-fiber green laser. (a) Output power as a function of the L for different R_2, and (b) the slope efficiency and laser threshold versus the L under $R_2 = 75\%$, $R_{2p} = 95\%$. (c) Output power versus the R_2 for different pump powers, and (d) the slope efficiency and laser threshold versus the R_2 under $L = 2$ m, $R_{2p} = 95\%$.

selected in high-power laser experiment. Figures 7(c) and 7(d) show the laser output power, slope efficiency, and threshold versus the R_2 under $L = 2$ m, $R_{2p} = 95\%$. It can be seen the output power first increases and then decreases with the reducing of R_2 under a fixed pump power. As the pump increases, the laser reflectivity R_2 for maximum power output decreases [see the dotted arrow in Fig. 7(c)]. As shown in Fig. 7(d), with the increase of R_2, the laser threshold and slope efficiency decrease. It is worth mentioning, however, that in DC Pr³⁺-doped fluoride fiber, the emission cross section of red light is substantially bigger than that of green light (i.e., the red gain is much stronger than that of green light). Even with only ~4% feedback at both ends

of the resonant cavity, red laser oscillation is easily formed under vigorous pumping. In practice, with the decrease of R_2 (i.e., the threshold of green laser increases), red laser oscillation may be established first in the Pr³⁺-doped fiber laser, resulting in the failure of green laser emission. Therefore, in designing the output mirror reflectivity of an all-fiber Pr³⁺-doped green laser, various factors (e.g., gain fiber length, output mirror transmittance in the red region) should be considered comprehensively to ensure the successful establishment of green laser oscillation. For example, in experiment, a ~2-m DC Pr³⁺-doped fluoride fiber was used, and the threshold of the red laser is about 1.6 W without the FDMs. According to the green laser threshold
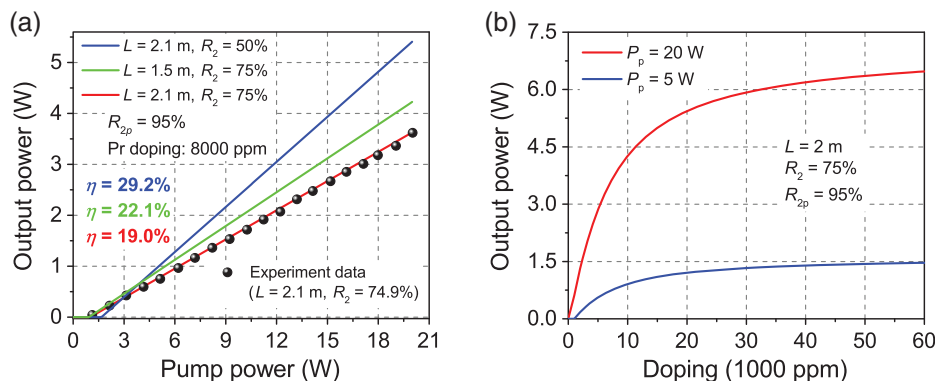
Fig. 8 (a) Green output power as a function of the pump power for different L and R_2. (b) Green output power versus the doping concentration of Pr³⁺ under $L = 2.0$ m, $R_{2p} = 95\%$.

in Fig. 7(d), it can be inferred that R_2 should be designed to be ~50% at this time to obtain higher efficiency and output power on the premise of the smooth establishment of the green laser.

We also carried out relevant simulations of the high-power all-fiber green laser with different optimization designs, and the results are shown in Fig. 8(a). For the $R_2 = 75\%$, varying the gain fiber from 2.1 to 1.5 m, both the green output power and slope efficiency increase from 3.63 to 4.23 W pumped at 20 W and from 19.0% to 22.1%, respectively. When the $L = 2.1$ m, with the R_2 decreasing from 75% to 50%, both the green output power and slope efficiency increase from 3.63 to 5.41 W pumped at 20 W and from 20.5% to 30.0%, respectively. Therefore, the output power and efficiency can be further improved by reasonably reducing the length of the gain fiber and increasing the green laser output coupling. Furthermore, as shown in Fig. 8(b), neglecting the loss caused by a higher doping level, it can be found that the green laser output power increases with the increase of the Pr³⁺ doping concentration, indicating that the output green laser power can also be further increased by increasing the Pr³⁺ doping concentration. In short, the numerical model well explains the experimental results of the all-fiber green laser [see the black sphere in Figs. 7(b), 7(d), and 8(a)], and predicts the potential of the visible DC Pr³⁺-doped all-fiber laser pumped by a standard multimode fiber-pigtailed blue LD.

4 Conclusions

A compact high-efficiency Watt-level CW all-fiber Pr³⁺-doped green laser pumped by a 443-nm fiber-pigtailed pump source was demonstrated. To achieve high-efficiency and high-power operation, the DC Pr³⁺-doped fluoride fiber connector was processed based on the cutting technology, and then the all-fiber green laser design was optimized using experiments and numerical simulations. According to the optimization results, we designed and demonstrated a compact high-power green all-fiber laser, which consists of a 2.1-m DC Pr³⁺-doped fiber, two homemade FDMs at visible wavelengths with a high damage intensity, and a 443-nm fiber-pigtailed pump source. The maximum output green laser power is up to 3.62 W at 521 nm, and the maximum slope efficiency is as high as 20.9%. To the best of our knowledge, this is the largest output power from the visible fiber lasers so far. Simulation performance of all-fiber green laser also shows that it is necessary to consider the optimum gain fiber length, output mirror reflectivity, and doping level. We believe the laser power scaling and slope efficiency could be further improved via (1) reducing the reflectivity of the output mirror at the laser wavelength, (2) uprating the power of 443 nm fiber-pigtailed pump laser, and (3) reducing the propagation loss and enhancing the doping level of DC Pr³⁺-doped fiber.

References

1. C. K. Sramek et al., "Therapeutic window of retinal photocoagulation with green (532-nm) and yellow (577-nm) lasers," *Ophthalmic Surg. Lasers Imaging Retina* **43**(4), 341–347 (2012).
2. L. Hu et al., "High-power hybrid GaN-based green laser diodes with ITO cladding layer," *Photonics Res.* **8**, 279–285 (2020).
3. G. K. Samanta, S. C. Kumar, and M. Ebrahim-Zadeh, "Stable, 9.6 W, continuous-wave, single-frequency, fiber-based green source at 532 nm," *Opt. Lett.* **34**, 1561–1563 (2009).
4. J. Liu et al., "Stable, 12 W, continuous-wave single-frequency Nd:YVO₄ green laser polarized and dual-end pumped at 880 nm," *Opt. Express* **19**, 6777–6782 (2011).
5. Y. Fujimoto, O. Ishii, and M. Yamazaki, "Multi-colour laser oscillation in Pr³⁺-doped fluoro-aluminate glass fibre pumped by 442.6 nm GaN-semiconductor laser," *Electron. Lett.* **45**(25), 1301–1302 (2009).
6. S. Ji et al., "Watt-level visible continuous-wave upconversion fiber lasers toward the "green gap" wavelengths of 535–553 nm," *ACS Photonics* **8**(8), 2311–2319 (2021).
7. J. Zou et al., "Green/red pulsed vortex-beam oscillations in all-fiber lasers with visible-resonance gold nanorods," *Nanoscale* **11**, 15991–16000 (2019).
8. H. Okamoto et al., "Visible–NIR tunable Pr³⁺-doped fiber laser pumped by a GaN laser diode," *Opt. Express* **17**, 20227–20232 (2009).
9. Y. Fujimoto et al., "Visible fiber lasers excited by GaN laser diodes," *Prog. Quantum Electron.* **37**(4), 185–214 (2013).
10. E. Kifle et al., "Watt-level visible laser in double-clad Pr³⁺-doped fluoride fiber pumped by a GaN diode," *Opt. Lett.* **46**, 74–77 (2021).
11. J. Zou et al., "Direct generation of watt-level yellow Dy³⁺-doped fiber laser," *Photonics Res.* **9**(4), 446–451 (2021).
12. W. Li et al., "High-efficiency broadband tunable green laser operation of direct diode-pumped holmium-doped fiber," *Opt. Express* **29**, 15564–15575 (2021).
13. M.-P. Lord et al., "2.3 W monolithic fiber laser operating in the visible," *Opt. Lett.* **46**, 2392–2395 (2021).
14. J. Zou et al., "Towards visible-wavelength passively mode-locked lasers in all-fibre format," *Light Sci. Appl.* **9**(1), 61 (2020).
15. H. Okamoto, K. Kasuga, and Y. Kubota, "Efficient 521 nm all-fiber laser: splicing Pr³⁺-doped ZBLAN fiber to end-coated silica fiber," *Opt. Lett.* **36**, 1470–1472 (2011).
16. J. Nakanishi et al., "High-power direct green laser oscillation of 598 mW in Pr³⁺-doped waterproof fluoroaluminate glass fiber excited by two-polarization-combined GaN laser diodes," *Opt. Lett.* **36**, 1836–1838 (2011).
17. J. Nakanishi et al., "Watt-order direct green laser oscillation at 522 nm in Pr³⁺-doped waterproof fluoro-aluminate-glass fiber," in *CLEO: 2013, CLEO: 2013*, Optica Publishing Group, p. JTu4A.02 (2013).
18. K. Fuwa and B. L. Valle, "The physical basis of analytical atomic absorption spectrometry. The pertinence of the Beer–Lambert law," *Anal. Chem.* **35**(8), 942–946 (1963).
19. E. C. Ji et al., "Spectroscopic properties of heavily Ho³⁺-doped barium yttrium fluoride crystals," *Chin. Phys. B* **24**(9), 094216 (2015).
20. M. Olivier et al., "Spectroscopic study and judd-ofelt analysis of Pr³⁺-doped Zr-Ba-La-Al glasses in visible spectral range," *J. Opt. Soc. Am. B* **30**, 2032–2042 (2013).
21. B. Aull and H. Jenssen, "Vibronic interactions in Nd:YAG resulting in nonreciprocity of absorption and stimulated emission cross sections," *IEEE J. Quantum Electron.* **18**(5), 925–930 (1982).
22. M. Amin, S. Jackson, and M. Majewski, "Experimental and theoretical analysis of Dy³⁺-doped fiber lasers for efficient yellow emission," *Appl. Opt.* **60**(16), 4613–4621 (2021).
23. I. Kelson and A. Hardy, "Strongly pumped fiber lasers," *IEEE J. Quantum Electron.* **34**(9), 1570–1577 (1998).

24. J. Shi et al., "Modeling and analysis of fiber Bragg grating based visible Pr³⁺-doped fiber lasers," *J. Lightwave Technol.* **32**, 27–34 (2014).
25. W. Wang et al., "Numerical analysis of 2.7 μm lasing in Er³⁺-doped tellurite fiber lasers," *Sci. Rep.* **6**, 31761 (2016).

Jinhai Zou received his BS degree in optoelectronic information science and engineering from China Jiliang University in 2017 and his PhD in electronic science and technology from Xiamen University in 2022. His research focuses on fiber lasers in the visible waveband.

Zhengqian Luo received his BS degree in applied physics from Harbin Institute of Technology in 2004 and his PhD in electrical engineering from Xiamen University in 2009. From 2007 to 2009, he studied at Nanyang Technological University as a joint PhD student. He joined Xiamen University as a faculty member in 2010. From 2016 to 2017, he was a visiting professor at Massachusetts Institute of Technology. Since 2017, he has been a full professor at Xiamen University and currently serves as the head of the Electronic Engineering Department of Xiamen University. His research focuses on ultrafast fiber lasers and on-chip photonic devices. He has published more than 150 journal or conference papers with total citations of >5500 times. He is a recipient of the National Science Fund for Excellent Young Scholars and the Fujian Youth Science and Technology Award. He is a senior member of IEEE and serves as a young editorial board member of Chinese Laser Press and associate director of the Optical Society of Fujian Province of China.

Biographies of the other authors are not available.